ACS APPLIED MATERIALS & INTERFACES

Research Article

www.acsami.org

Antifungal Coatings Based on $Ca(OH)_2$ Mixed with ZnO/TiO_2 Nanomaterials for Protection of Limestone Monuments

Nikte Gómez-Ortíz,*[,†] Susana De la Rosa-García,[‡] William González-Gómez,[†] Montserrat Soria-Castro,[†] Patricia Quintana,[†] Gerko Oskam,[†] and Benjamin Ortega-Morales[‡]

[†]Departamento de Física Aplicada, CINVESTAV-IPN, A.P. 73, Cordemex, Mérida, Yucatán 97310, México

[‡]Departamento de Microbiología Ambiental y Biotecnología, Universidad Autónoma de Campeche, Avenida Agustín Melgar s/n, Campeche, Campeche 24039, México

Supporting Information

ABSTRACT: The presence and deteriorating action of microbial biofilms on historic stone buildings have received considerable attention in the past few years. Among microorganisms, fungi are one of the most damaging groups. In the present work, antimicrobial surfaces were prepared using suspensions of $Ca(OH)_2$ particles, mixed with ZnO or TiO_2 nanoparticles. The antimicrobial surfaces were evaluated for their antifungal activity both in the dark and under simulated natural photoperiod cycles, using *Penicillium oxalicum* and *Aspergillus niger* as model organisms, and two limestone lithotypes commonly used in construction and as materials for the restoration of historic buildings. Both $Ca(OH)_2$-ZnO and $Ca(OH)_2$-TiO_2 materials displayed antifungal activity: ZnO-based systems had the best antifungal properties, being effective both in the dark and under illumination. In contrast, TiO_2-based coatings showed antifungal activity only under photoperiod conditions. Controls with coatings consisting of only $Ca(OH)_2$ were readily colonized by both fungi. The antifungal activity was monitored by direct observation with microscope, X-ray diffraction (XRD), and scanning electron microscopy (SEM), and was found to be different for the two lithotypes, suggesting that the mineral grain distribution and porosity played a role in the activity. XRD was used to investigate the formation of biominerals as indicator of the fungal attack of the limestone materials, while SEM illustrated the influence of porosity of both the limestone material and the coatings on the fungal penetration into the limestone. The coated nanosystems based on $Ca(OH)_2$-50%ZnO and pure zincite nanoparticulate films have promising performance on low porosity limestone, showing good antifungal properties against *P. oxalicum* and *A. niger* under simulated photoperiod conditions.

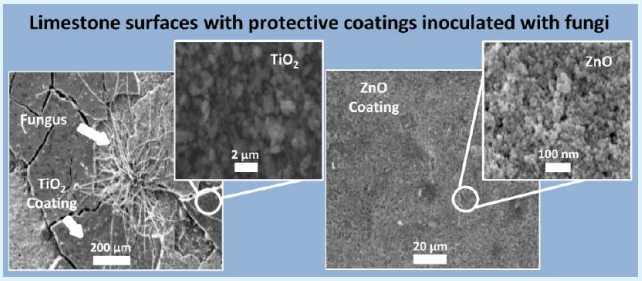

KEYWORDS: *antimicrobial surfaces, $Ca(OH)_2$ particles, ZnO nanoparticles, TiO_2 nanoparticles, Penicillium oxalicum, Aspergillus niger*

1. INTRODUCTION

Archaeological and historic stone monuments, statues, and stelae are exposed to the effects of physical, chemical, and biological deterioration factors. Among biological factors, microbial biofilms are a major cause of stone decay. Colonization can occur both on the surface (epilithic growth), usually the predominant form of microbial colonization in Mayan buildings,[1,2] and inside the stone in cracks, crevices or bored microholes.[3] Biodeterioration of stone monuments and buildings is a well-recognized problem in tropical regions.[1,4] The climate of the Yucatán peninsula is characterized by high temperatures and solar radiation intensity throughout most of the year. In addition, a high relative humidity and rainfall favor the growth of a wide variety of living microorganisms on stone surfaces.[5] Limestone is an extensively used building material, which is highly susceptible to deterioration by organic acids and water.

Stone monuments can be colonized by different groups of microorganisms, including bacteria, algae, and fungi.[6] Fungi are very active biological agents that can colonize a wide variety of materials with different physical characteristics, where porosity, roughness and permeability play an important role. Hence, there is a need to increase our understanding of the influence of petrographical and physicochemical properties on biological colonization.[6,7] The deterioration of marble, limestone, granite, and basalt by filamentous fungi through the action of excreted organic acids such as oxalic and citric acid has been reported in the literature.[8−10] It has also been shown that fungal species such as *Aspergillus niger* were able to solubilize powdered stone and chelate minerals in a glucose-rich medium due to the production of organic acids such as gluconic, citric, and oxalic

Received: March 23, 2012
Accepted: January 24, 2013
Published: January 24, 2013

acid.[10,11] Similar experiments involving limestone have demonstrated the formation of oxalate crystals upon the reaction with oxalic acid, which adhered to fungal hyphae.[12] Biocide coatings to prevent biodeterioration have been investigated, but their performance has not been optimal. Fungal growth has been difficult to control because fungi have developed resistance to conventional fungicides, and the potential health risk to humans and animals has led to the development of new methods for the conservation of materials for cultural heritage applications using surface modification with antimicrobial materials.[6,13−15] Nanoparticulate oxide materials are attractive because of their unique physical and chemical properties, and show promise for the development of an environmentally responsible method for preventing biodeterioration of building materials.[16−19]

Calcium hydroxide, $Ca(OH)_2$, is one of the most interesting products for consolidation of calcareous-based stone sculptures, monuments or even wall paintings.[20] Its low solubility and physicochemical properties compatible with stone surfaces favor its use in limestone-based conservation treatments.[15,21−23] Baglioni and Giorgi synthesized nanoparticles in nonaqueous solvents with optimal properties for application to cultural heritage conservation, as was demonstrated in the protection of stucco coatings in the archeological ruins of Calakmul, in Campeche, México.[17] However, the authors did not determine the antimicrobial properties of this nanosystem. Inorganic metal oxides such as TiO_2, MgO, CaO, and ZnO have also attracted interest as antimicrobial agents because of their safety and stability. Among these, ZnO nanostructures are at the forefront of research due to their unique properties and widespread applications. Antibacterial properties of pure ZnO,[24,25] ZnO−CaO solid solutions,[26] and mixtures of ZnO and MgO powders,[27] have been reported. It has been shown that ZnO nanoparticles have selective toxicity toward bacteria, and thanks to its biocompatible properties, it has been used as drug delivery material, cosmetic ingredient, and medical filling material.[28,29] It has been suggested that nano-ZnO could be used as an effective fungicide for preserving agricultural products given its excellent antibacterial activity when deposited on cotton fabrics and food.[30,31] Because ZnO nanoparticles possess antibacterial and antifungal activities at low concentrations[32] with low cytotoxicity, ZnO-based nanosystems are promising as preventive and remedial coatings on calcareous stone. The anatase phase of TiO_2 is an attractive material for a large variety of applications, such as sensors,[33] photocatalysts,[34,35] controlled drug release material,[36] and dye-sensitized solar cells,[37] related to its chemical stability, nontoxic properties, and stability under UV light.[33−39] Moreover, anatase has been reported to be a better agent for preventing biodeterioration because of some microalgae and cyanobacteria than conventional biocides including Biotin T and Anios D.D.S.H.[38,39]

In this work, we report on the preparation of antifungal coatings based on $Ca(OH)_2$ mixed with ZnO and TiO_2 nanomaterials both on glass slides and on two types of limestone. The antifungal activity was determined both in the dark and under illumination, using *Penicillium oxalicum* and *Aspergillus niger* as model organisms.

2. EXPERIMENTAL METHODS

2.1. Synthesis and Characterization of Metal Oxide Materials. $Ca(OH)_2$ was synthesized according to the method reported by Ambrosi[20] as follows: 100 mL of 0.8 M NaOH solution (Aldrich, 98+%) and 100 mL of 0.4 M $CaCl_2{\cdot}H_2O$ (Reasol, 78%) were separately heated to 80 °C, and were mixed under stirring. The reaction mixture was cooled under a nitrogen atmosphere, and the resulting suspension was washed five times with water (Labconco WaterPro PS; 18 MΩ cm) to remove NaCl. Nanoparticulate ZnO was synthesized from denatured ethanol (J.T. Baker, 99.6%) using 100 mL of 65 mM NaOH (Aldrich, 98+%) and 100 mL of 40 mM zinc acetate dihydrate ($Zn(CH_3COO)_2{\cdot}2H_2O$) (Aldrich, 98+%) at 60 °C. The two solutions were mixed and kept at that temperature for 5 h with vigorous stirring. Subsequently, 6.6 mL of 2.2 M $Zn(CH_3COO)_2{\cdot}2H_2O$ and 6.6 mL of 3.6 M NaOH, both water-based solutions, were added to the solution. The reaction mixture was stirred for 14 h at room temperature. Finally, the solution was centrifuged and washed with acetone (J.T. Baker, 99.8%): water with a volume ratio of 6:3. The coating suspension was prepared by adding different amounts of ZnO nanomaterial to 200 mL of 0.27 M $Ca(OH)_2$ in ethanol in order to obtain suspensions of 10, 30, and 50 wt % ZnO, respectively.

Titanium dioxide (TiO_2) nanoparticles were synthesized according to the method reported by Burnside et al.[40] as follows: 162 mL of titanium(IV) isopropoxide (Aldrich, 97%) was rapidly added to 290 mL of distilled water and stirred for 1 h. The resulting suspension was filtered using a glass frit and washed three times with 50 mL of distilled water. The filter cake was treated in an autoclave containing 30 mL of 0.6 M tetramethylammonium hydroxide solution at a temperature of 150 °C for 6 h, until a white slurry was formed with a pH between 7 and 8. The slurry was treated under reflux conditions for 3−6 h under ambient pressure conditions at about 100 °C in order to break the large agglomerates into smaller aggregates and primary particles, and turned into a translucent blue-white suspension. The resulting colloidal suspension was treated hydrothermally in the autoclave at 200 °C during 4.5 h. Finally, the solution was centrifuged and washed with acetone:water with a volume ratio of 7:3, 6:4, and 1:1. The coating suspension was prepared by adding different amounts of TiO_2 nanomaterial to 200 mL of 0.27 M $Ca(OH)_2$ in ethanol in order to obtain suspensions of 10, 20, and 30 wt % TiO_2, respectively.

The phase composition of specimens was analyzed using X-ray diffraction (XRD Siemens D-5000), with a Bragg−Brentano geometry and Cu−Kα radiation (λ = 1.5418 Å) using the following scan: step size = 0.02°, t = 5 s, 5° ≤ 2θ ≤ 70°. The crystallite size, r, was obtained using the Scherrer equation for the peak width according to

$$r = \frac{0.9\lambda}{2B\cos\theta} \quad (1)$$

where B is the peak width (fwhm; in radians) corrected for the instrument broadening, determined from the spectra of the same materials with large crystallite size, using an error-type quadratic correction with B_{ins} = 2.9 × 10^{-3} rad, λ = 0.154 nm, and θ is the reflection angle.[41,42] Phase analysis was realized before and after fungal colonization. The nanoparticle size was corroborated with high-resolution scanning electron microscopy (HR-SEM, Jeol JSM-7600F). The morphology and deterioration of the stone specimens by hyphae penetration was analyzed by SEM (Phillips XL30 ESEM) (1 to 30 kV) coupled to an energy-dispersive spectrometer (EDS) at 25 kV, and with an optical microscope (Labtronic Scientific, DIN-125) coupled to a white and yellow illuminator (Fiber-Lite MI-150 Gooseneck Systems, Dolan-Jenner).

2.2. Culture and Preparation of Inocula of *Penicillium oxalicum* and *Aspergillus niger*. The fungus *Aspergillus niger* Van Tieghem (ATCC 16888) was purchased from the American Type Culture Collection; this particular fungus is a very active producer of various types of organic acid. *Penicillium oxalicum* Currie & Thom (TM1H52) was isolated from stones with a black biogenic surface from the Chichén Itza area, and was shown to be especially active in solubilizing calcium carbonate plates and limestone coupons through the production of oxalic and citric acids. Fungal inoculum was prepared by growing *A. niger* and *P. oxalicum* on potato dextrose agar (PDA, Difco) plates at 27 °C for four days. Fungal growth from plates was flooded with sterile saline solution (0.85%) with 0.2% of Tween 80 (v/v) and stirred gently with a sterile swab. The resulting suspension of each fungus was drawn off with a pipet, and then

transferred to a clean tube. The concentrations of spore in the stock suspensions were determined using a Neubauer counter chamber and were adjusted to 1×10^6 spores/mL in malt extract broth (Fluka) amended with glucose (5%).

2.3. Determination of Antifungal Activity of $Ca(OH)_2$-ZnO and $Ca(OH)_2$-TiO_2 Nanosystems. The antifungal activity of the $Ca(OH)_2$, $Ca(OH)_2$-xZnO, and $Ca(OH)_2$-$x$$TiO_2$ nanosystems was tested in vitro using two types of substrate: (i) glass microscope slides; and (ii) limestone coupons of two different lithotypes. The $Ca(OH)_2$-xZnO nanosystem was applied to microscope slides with different amounts of ZnO (x = 10, 30, or 50 wt %), and compared to the pure ZnO and $Ca(OH)_2$ systems; all samples were prepared in triplicate. The $Ca(OH)_2$ - $x$$TiO_2$ mixtures were also tested at three levels of TiO_2 (x = 10, 20, and 30 wt %). The $Ca(OH)_2$ coating was tested specifically as a reference nanosystem for cultural heritage applications.[17] A negative control consisting of an uncoated slide was also included.

Microscope slides were cleaned ultrasonically first with an Alconox powder detergent solution for 30 min, and then with a mixture of 2-propanol-water (1:1). Slides were heated to 60 °C on a hot plate, and were then coated using the different systems by dropwise addition of 4 mL of the suspensions in a period of 2 min. After allowing the covered slides to dry, 1 mL of well-stirred fungal inocula (1×10^6 spores/mL) was applied to an area of 4 cm^2 of the sample using a micropipet, which was sufficient to cover the sample area. The homogeneity of the spore distribution was verified using optical microscopy.

The slides were separated into two groups; one group was incubated at 27 °C in the dark (D) in a bacteriological incubator at 80% RH (relative humidity), whereas the other group was subjected to conditions simulating a natural photoperiod (D/NL). The simulated photoperiod consisted of daily cycles with 12 h of darkness and 12 h of illumination with natural light, which was achieved by placing the samples in a glass Petri dish on a window sill; note that the glass windows absorb a significant portion of the UV light in the solar spectrum. Fungal growth was inspected daily using a stereoscopic microscope (Nikon) for 120 h. The inspection consisted of visual counting of colonies in the Petri dish divided in sections of 1 cm^2. Antifungal activity of the treatments was noted as (+++) effective, when no hyphae or mycelium were observed on the surface and only spores left over from the inoculation step were present; (++) moderate, corresponding to a surface coverage with fungi of less than 25%; (+) poor, corresponding to a surface coverage with fungi between 25% and 75%; and (−) ineffective, corresponding to a coverage of 75% to 100%. In vitro fungal growth was compared with a control glass side without a coating. The results of these experiments served as guidance for the design of the experiments on limestone samples.

The limestone materials were obtained either from a quarry in the Chichén Itza region (Yucatán, México) or from local building industry suppliers, and were selected considering their regional significance, abundance and frequency of usage as a building and restoration material. The limestone materials were cut into coupons (2 cm × 2 cm × 1 mm) employing a low-speed diamond saw. Coupons were sterilized using UV light exposure for 48 h, then autoclaved at 121 °C for 6 h, and finally dried inside an oven at 115 °C for 24 h;[43] performing the pretreatment steps in this specific order has been shown to warrant an optimal sterility of rock specimens.[44] Limestone coupons were covered with the antifungal coatings by submerging the samples individually in the coating material suspensions, and subsequently placing the container in an ultrasonic bath for 5 min in order to ensure complete coverage of the irregular limestone surface. During the ultrasonic treatment, the temperature of the coating suspension increased, resulting in partial evaporation of the ethanol solvent, thus assisting the deposition process. The samples were allowed to dry at room temperature and were sterilized again under UV for 24 h, after which a predetermined volume sufficient to cover the sample surface of 1 mL of the fungal spore suspension was applied to the coated surfaces using a micropipet, and the homogeneity of the spore distribution was verified using optical microscopy. Antifungal activity was tested as follows: samples were incubated at 27 °C in a bacteriological incubator at 80% RH under a simulated photoperiod (D/UVL) consisting of daily cycles of 12 h in the dark and 12 h under UV illumination (Source Light GPH357T5/VH; 17 W; 185 - 330 nm) for 21 days. Note that the shortest wavelength range of the UV light was removed by employing a plastic Petri dish lid as an optical filter (185 nm −305 nm) in order to protect the fungi. Antifungal activity of the treatments was noted as (+++) effective; (++) moderate; (+) poor; and (−) ineffective, defined as described above for the coated glass substrates.

3. RESULTS AND DISCUSSION

3.1. Characterization of Metal Oxide Nanomaterials for Antifungal Coatings. X-ray diffraction patterns of the products from the synthesis of $Ca(OH)_2$ material mainly consists of portlandite (curve a), whereas the ZnO and TiO_2 nanomaterials are pure zincite (curve b) and anatase (curve c), respectively, as shown in Figure 1. The average crystallite size

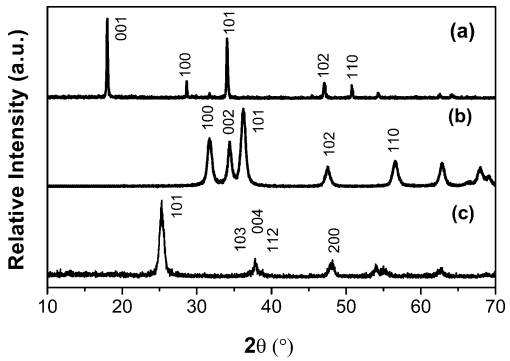

Figure 1. X-ray diffraction patterns of the nanomaterials synthesized: (a) $Ca(OH)_2$; (b) ZnO; (c) TiO_2. The reference patterns correspond to the JCPDS: (a) No 04−0733, (b) No 36−1451, and (c) No 21−1276, respectively.

can be obtained from the peak width, for nanocrystallites smaller than about 50 nm,[41] according to the Scherrer equation (eq 1). In the case of zincite, the crystallite diameter is in the range of 26 nm, whereas anatase nanocrystallite have an average diameter of 14 nm. The sharp peaks obtained for the $Ca(OH)_2$ portlandite phase indicate that the crystallite size is larger than 50 nm.

Figure 2 shows SEM images of the $Ca(OH)_2$, ZnO, and TiO_2 nanoparticles: the $Ca(OH)_2$ material consist of hexagonal flakes of around of 500 nm in size, whereas ZnO consists of spherical nanoparticles of around of 10 - 30 nm, and TiO_2 of faceted nanoparticles of less than 50 nm in diameter, respectively.

3.2. Antifungal Activity of Coatings on Glass Slide Substrates. Growth inhibition of *A. niger* and *P. oxalicum* was examined on nanoparticulate coatings on glass slides containing a range of concentrations of different systems, both in the dark and under the simulated photoperiod conditions. The coated glass slides were exposed to the fungi for 120 h. It was observed that the growth of *P. oxalicum* was slightly more inhibited than that of *A. niger,* both in the dark and under natural photoperiod conditions (Tables 1 and 2).

The $Ca(OH)_2$ system showed a moderate antifungal activity under natural photoperiod conditions for both fungi. Without illumination, only *P. oxalicum* exhibits moderate inhibition for up to 72 h and afterward the effectiveness of the coating was minimal. The $Ca(OH)_2$ system has a basic pH that reduces the growth of fungi (Table 2), because it is a good deacidifying agent.[17] However, upon adding the more acidic TiO_2

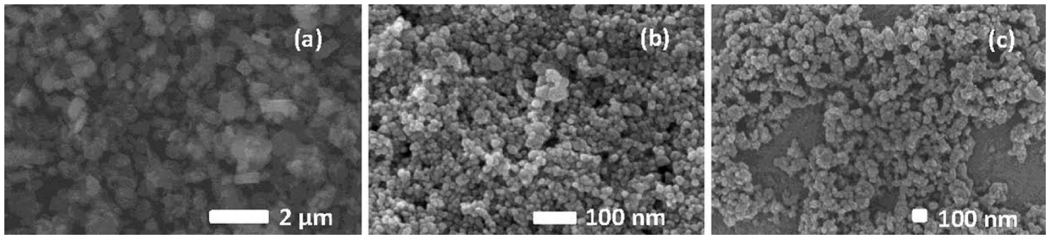

Figure 2. Scanning electron microscopy images of: (a) $Ca(OH)_2$ particles that form the basis for the antifungal coatings, (b) ZnO nanoparticles, and (c) TiO_2 nanoparticles.

Table 1. Antifungal Activity for Coatings on Glass Slides in the Dark (D)[a]

	time (h)					
	A. niger			*P. oxalicum*		
	24	72	120	24	72	120
control (untreated)	(−)	(−)	(−)	(−)	(−)	(−)
Ca $(OH)_2$	(−)	(−)	(−)	(++)	(++)	(−)
Ca $(OH)_2$-10% TiO_2	(−)	(−)	(−)	(−)	(−)	(−)
Ca $(OH)_2$-20% TiO_2	(−)	(−)	(−)	(−)	(−)	(−)
Ca $(OH)_2$-30% TiO_2	(−)	(−)	(−)	(−)	(−)	(−)
ZnO	(+++)	(+++)	(+++)	(+++)	(+++)	(+++)
Ca $(OH)_2$-10% ZnO	(+++)	(+++)	(++)	(+++)	(+++)	(+++)
Ca $(OH)_2$-30% ZnO	(+++)	(+++)	(++)	(+++)	(+++)	(+++)
Ca $(OH)_2$-50% ZnO	(+++)	(+++)	(+++)	(+++)	(+++)	(+++)

[a](+++) effective (++) moderate, (+) poor (−) ineffective.

Table 2. Antifungal Activity of Coatings on Glass Slides under Natural Photoperiod Conditions (D/NL)[a]

	time (h)					
	A.niger			*P. oxalicum*		
	24	72	120	24	72	120
control (untreated)	(−)	(−)	(−)	(−)	(−)	(−)
Ca $(OH)_2$	(++)	(++)	(++)	(++)	(++)	(++)
Ca $(OH)_2$-10% TiO_2	(++)	(+)	(−)	(++)	(++)	(++)
Ca $(OH)_2$-20% TiO_2	(++)	(+)	(+)	(++)	(++)	(++)
Ca $(OH)_2$-30% TiO_2	(++)	(+)	(+)	(++)	(++)	(++)
ZnO	(+++)	(+++)	(+++)	(+++)	(+++)	(+++)
Ca $(OH)_2$-10% ZnO	(++)	(++)	(++)	(+++)	(+++)	(+++)
Ca $(OH)_2$-30% ZnO	(+++)	(+++)	(++)	(+++)	(+++)	(+++)
Ca $(OH)_2$-50% ZnO	(+++)	(+++)	(+++)	(+++)	(+++)	(+++)

[a](+++) effective (++) moderate, (+) poor (−) ineffective.

nanomaterial, the weak antifungal activity disappears: $Ca(OH)_2TiO_2$ treatments were ineffective in terms of antifungal activity under dark conditions (Table 1). Under the natural photoperiod treatment, a moderate to poor inhibition was observed with increasing exposure time with *A. niger* (Table 2), whereas in the case of *P. oxalicum*, the moderate antifungal activity was constant, independent of the amount of TiO_2 and the exposure time. The limited antifungal activity could be related to the relatively low intensity of UV light used in these experiments behind glass windows, hence, a better performance may be expected under direct sun light.[47] Moreover, it has been reported that TiO_2 is a better agent for preventing biodeterioration than conventional biocides when used against lichens, bacterial and other phototrophic microorganism.[45,46] On the other hand, the antifungal effectiveness of the $Ca(OH)_2$-*x*ZnO nanosystem increases with the amount of the more basic oxide ZnO, related to the general observation that fungal growth is inhibited in basic media.[17] Furthermore, no germination of spores for both fungi was observed when pure ZnO was applied and, therefore, there is no presence of mycelium, which are typical structures of the fungi.

On the basis of these results, four different systems were selected to be applied onto two different limestone coupons: $Ca(OH)_2$-50% TiO_2, pure TiO_2, $Ca(OH)_2$-50% ZnO, and pure ZnO.

The different coatings on glass slides were analyzed by XRD before and after the inoculation treatment (Figure 3a), in order to characterize the changes in composition related to the interaction of the fungi with the consolidated materials. The $Ca(OH)_2$ coating, before interaction with the fungi, mainly

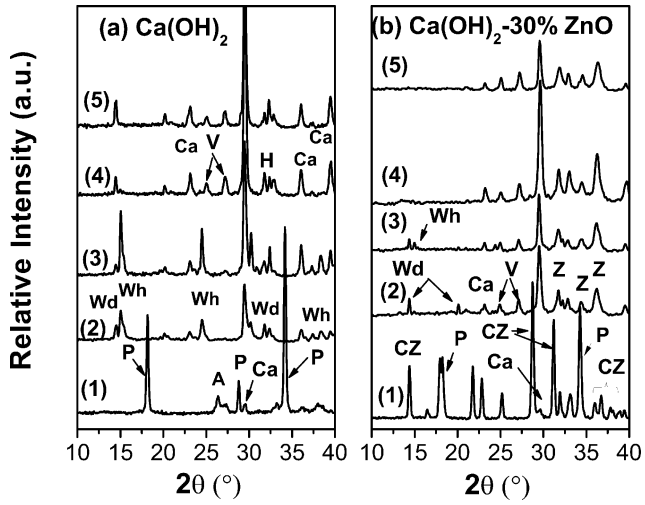

Figure 3. X-ray patterns of the nanosystem coatings on glass slides before and after inoculation with *P. oxalicum* or *A. niger* after 120 h either in the dark (D) or under natural photoperiod conditions (D/NL): (a) pure $Ca(OH)_2$; (b) $Ca(OH)_2$-30%ZnO. For both figures: (1) glass slide with the coating before inoculation; (2) coating after inoculation with *P. oxalicum* (D); (3) coating after inoculation with *P. oxalicum* (D/NL); (4) coating after inoculation with *A. niger* (D); (5) coating after inoculation with *A. niger* (D/NL). The phases/materials observed were: calcite (Ca), aragonite (A), portlandite (P), vaterite (V), whewellite (Wh), weddellite (Wd), zincite (Z), and calcium zincate dihydrate (CZ).

dx.doi.org/10.1021/am302783h | ACS Appl. Mater. Interfaces 2013, 5, 1556−1565

consists of the portlandite (P) phase, together with small amounts of calcium carbonate polymorphs, $CaCO_3$, such as calcite (C) and aragonite (A). After inoculating the $Ca(OH)_2$ coating with *P. oxalicum,* mainly calcite was obtained with the presence of small amounts of two calcium oxalates: the monohydrate $C_2CaO_4{\cdot}H_2O$, known as a whewellite (Wh) and the dihydrate, weddellite (Wd). On the other hand, with *A. niger* the main phase was calcite, and small amounts of another polymorph of calcium carbonate named vaterite (V) as well as Wd were present. It can be observed that $Ca(OH)_2$ coated glass slides show a larger presence of calcium oxalates when inoculated with *P. oxalicum* than with *A. niger*. It can be concluded that, when the coatings are used for antifungal protection of historic monuments, the interaction of fungi with $Ca(OH)_2$ gives rise to the appearance of new phases, which may differently affect the stability of limestone surfaces, altering and somewhat passivating the surface itself.[48] Coatings of mixed $Ca(OH)_2$-*x*ZnO systems with a low amount of ZnO (10%), show the presence of portlandite and a small amount of zincite before inoculation. When the proportion of ZnO increases to 30% (Figure 3b), calcium zincate dihydrate (CZ) is formed with a chemical formula $Ca(Zn(OH)_3)_2{\cdot}2H_2O$.[48] This compound plays an important role in the retardation of cement hydration and in the passivation of galvanized metals.[49,50] In all cases, calcite is detected as well.

Under dark conditions (D), inoculation with *P. oxalicum* results in an increasing calcite and decreasing vaterite content with increasing ZnO concentration, with vaterite being absent in the samples with 50% ZnO. The Wd phase is observed for the coatings with 10 and 30% ZnO, whereas Wh is only present with 30% ZnO. These compounds are not formed in the system with 50% ZnO. With the simulated photoperiod treatment an opposite trend is observed, where the amount of calcite diminishes and that of vaterite increases with the increasing amount of ZnO. Both calcium oxalates, Wd and Wh, are formed with 10% ZnO and their presence diminishes with 30% ZnO content, while at higher amounts of ZnO these phases are not detected. When the coatings were inoculated with *A. niger* with the two types of treatment, similar phase behavior was observed. The only difference was that with D/NL cycles, the formation of calcium oxalates was not favored. In the Supporting Information (Figure S1), a semiquantitative X-ray analysis is shown, illustrating the dependence of the observed phase composition for both dark and simulated photoperiod treatments of $Ca(OH)_2$-*x*ZnO coating materials, after inoculation with both fungi. In the case of pure ZnO coatings, only the presence of zincite (Z) is observed, both before and after the inoculation with both types of fungus, hence, the fungi are not capable of transforming ZnO to other materials.

3.3. Limestone Surfaces and Biofilm Formation. *3.3.1. Characterization of Limestone Materials and the Effect of Biofilm Formation.* The two types of limestone used in this work represent regional materials that were and still are used for construction, and for restoration of stone historic monuments. The physical properties of both types of limestone are summarized in Table 3, where it can be observed that the porosity of limestone A is almost 5 times higher than that of limestone type B. This difference in porosity is expected to significantly affect the stability of the material upon attack of fungi, and is an important parameter to have in mind when investigating biofilm formation on stone surfaces.

Table 3. Physical Properties of Two Limestone Materials,[51] Determined According to UNE-EN and ISRM Norms[53]

physical properties	limestone A	limestone B	NORM
water content (%)	0.12	0.03	UNE-EN 1936:1999, RILEM 1980[53]
water absorption (%)	6.59	1.22	UNE-EN 13755:2001, NORMAL 7/81[53]
density (g/cm^3)	2.18	2.55	ISRM 1979[53]
effective porosity (%)	6.16	1.27	ISRM 1981, TSE, 1987[53]

The limestone coupons were analyzed by powder XRD. Calcite was the main phase for limestone coupon, with traces of other minerals such as magnesium carbonates, hydrated calcium and magnesium sulfates and quartz. To detect phases other than calcite, powder obtained from grinding limestone samples was treated with 5% HCl to dissolve the carbonates and sulfates. Figure 4 shows the XRD spectra after the HCl

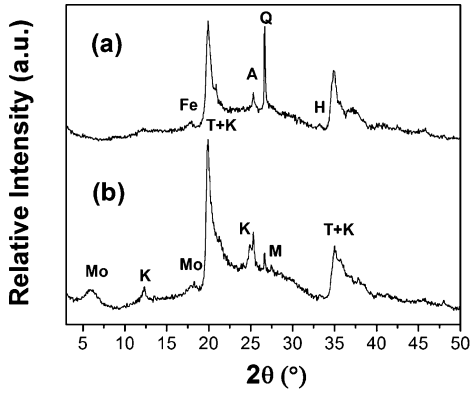

Figure 4. XRD patterns for limestone coupons after the dissolution of carbonate compounds with HCl (5% v/v). Fe = iron oxyhydroxides, A = anatase, Q = quartz, H = hematite, Mo = smectite, K = kaolinite, T = tosudite, and M =microcline.

treatment for the two materials. Limestone material B contains small amounts of feldspars such as microcline ($KAlSi_3O_8$), clays such as tosudite ($Na_{0.5}(Al,Mg)_6(Si,Al)_8O_{18}(OH)_{12}{\cdot}5H_2O$), kaolinite ($Al_2Si_2O_5(OH)_4$) and smectite ($Ca_{0.2}(Al,Mg)_2Si_4O_{10}(OH)_2{\cdot}4H_2O$), as well as oxides, including anatase (TiO_2). Limestone type A also contains tosudite and kaolinite, and contains apart from anatase, also iron oxyhydroxide (FeO(OH)), hematite (Fe_2O_3), and quartz. In addition, it was found that lithotype A contains a larger number of magnesium compounds (carbonates and sulfates, not shown in the figure) than lithotype B.

A set of limestone coupons without any protective coatings were monitored during biological incubation for 21 days with illumination cycles of D/UVL. After this time, the limestone coupons were found to be completely covered with a thin biofilm. The macroscopic appearance of the biofilms was corroborated by the presence of green and dark spores, typical of *P. oxalicum* and *A. niger* organisms, respectively. The biofilms were easily removed from the limestone coupon with a toothbrush, except for coupon B when *P. oxalicum* was cultivated: since the biofilm was strongly attached to the limestone surface, it was necessary to use a scalpel to remove the film. The effects of fungal growth on the limestone surfaces were analyzed with an optical microscope after removing the

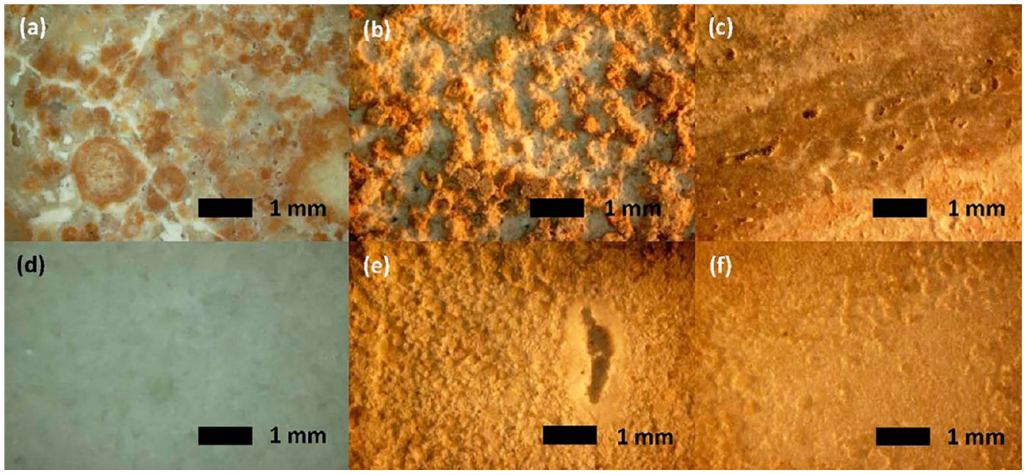

Figure 5. Optical microscope images (4.5×), obtained using illumination with yellow light: (a) surface of natural limestone coupon A; (b) limestone coupon A surface after removing the biofilm that resulted from culture with *P. oxalicum*; (c) limestone coupon A surface after removing the biofilm that resulted from culture with *A. niger*; (d) surface of natural limestone coupon B; (e) limestone coupon B surface after removing the biofilm that resulted from culture with *P. oxalicum*; and (f) Limestone coupon B surface after removing the biofilm that resulted from culture with *A. niger*.

biofilm, and compared with the natural limestone coupon as shown in Figure 5. When *P. oxalicum* is applied on limestone coupon A, a rough surface is observed indicating the deterioration of the stone by interaction with the fungus. The iron oxide patches of coupon A were more stable against deterioration than the areas where silicates predominate. Meanwhile, for limestone coupon B, a more homogeneous roughness is detected with observable porosity due to the interaction with the fungus. With *A. niger* on limestone coupon A, a less heterogeneous surface is obtained, whereas for limestone coupon B, a smooth and homogeneous texture is observed.

3.3.2. Characterization of Inoculated Stone Surfaces with Antifungal Coating. On the basis of the results obtained on glass slides, the following coating systems were chosen to be applied to the limestone substrates in order to characterize their antifungal properties: $Ca(OH)_2$-50% TiO_2, pure TiO_2, $Ca(OH)_2$-50% ZnO, and pure ZnO. The limestone coupons were inoculated with the two fungi and submitted to the D/UVL photoperiod treatment. The results of the antifungal activity are shown in Table 4. Without antifungal coating, the limestone substrates were completely covered with a biofilm after 2 days. It was observed that the effectiveness of the antifungal coatings was the best for formulations containing ZnO and $Ca(OH)_2$-50% ZnO. Pure TiO_2 and $Ca(OH)_2$-50% TiO_2 were moderately effective after 21 days of exposure to *P. oxalicum*, whereas the coatings were less effective upon exposure to *A. niger*. These results indicate that TiO_2 is less active as an antifungal material than ZnO, even under illumination, in agreement with the results on glass slides.

Table 4. Antifungal Activity of Coatings Applied to Two Different Limestone Coupons after 21 Days of Exposure under Simulated Photoperiod (D/UVL)[a]

	limestone coupons			
	A		B	
coating composition	*A. niger*	*P.oxalicum*	*A. niger*	*P.oxalicum*
control (untreated)	$(-)^2$	$(-)^2$	$(-)^2$	$(-)^2$
$Ca(OH)_2$-50%TiO_2	$(+)^{14}$	(+++)	$(++)^6$	(+++)
TiO_2	$(++)^6$	$(++)^{16}$	$(+)^{12}$	(+++)
$Ca(OH)_2$-50%ZnO	(+++)	(+++)	(+++)	(+++)
ZnO	(+++)	(+++)	(+++)	(+++)

[a](+++) effective (++) moderate, (+) poor (−) ineffective.

The superscript in Table 4 shows for how many days after inoculation the antifungal activity decreased with time, while a constant activity observed after this day for up to 21 days; this situation corresponds to a steady state in the number of observed colonies. Note that for the control coupons, the samples were completely covered with colonies after 2 days.

After 6−16 days, depending on the coating, the number of colonies remained essentially the same, indicating a steady state situation determined by the prevention of new colonies related to the antifungal activity.

XRD spectra of both limestone coupons after the inoculation with *A. niger* and *P. oxalicum* without the antifungal coatings, as illustrated in Figure 6 curve (1), mainly show the presence of calcite and weddellite, except for coupon B with *P. oxalicum*, where a small amount of whewellite was also detected. The portlandite peak is not observed, indicating that after 21 days all $Ca(OH)_2$ is converted. The presence of weddellite and whewellite indicates that the interaction of the fungi with the limestone can include the formation of biominerals derived from the reaction of organic acids with cations released from the limestone Figure S2 (see the Supporting Information). Frequently, calcium oxalate deposits have been found in crusts taken from weathering monuments, and in many cases their presence is associated with fungal activity.[52]

X-ray diffraction was also performed after the inoculation test on the limestone coupons, previously coated with either $Ca(OH)_2$-50% TiO_2 or $Ca(OH)_2$-50% ZnO. In general, for both coupons, the peak intensities corresponding to Wd and Wh are much lower for the coated limestone samples than for the uncoated samples, which reflects the antifungal properties of the coatings. For limestone coupon A, peaks corresponding to Wd and Wh are essentially absent for both the $Ca(OH)_2$-50% ZnO and the $Ca(OH)_2$-50% TiO_2 coatings, for both *A. niger* and *P. oxalicum*. For limestone coupon B, a small Wd signal is observed for the sample inoculated with *A. niger* with the $Ca(OH)_2$-50% ZnO coating, indicating that the coating is not completely effective. On the other hand, a Wd signal is

dx.doi.org/10.1021/am302783h | ACS Appl. Mater. Interfaces 2013, 5, 1556−1565

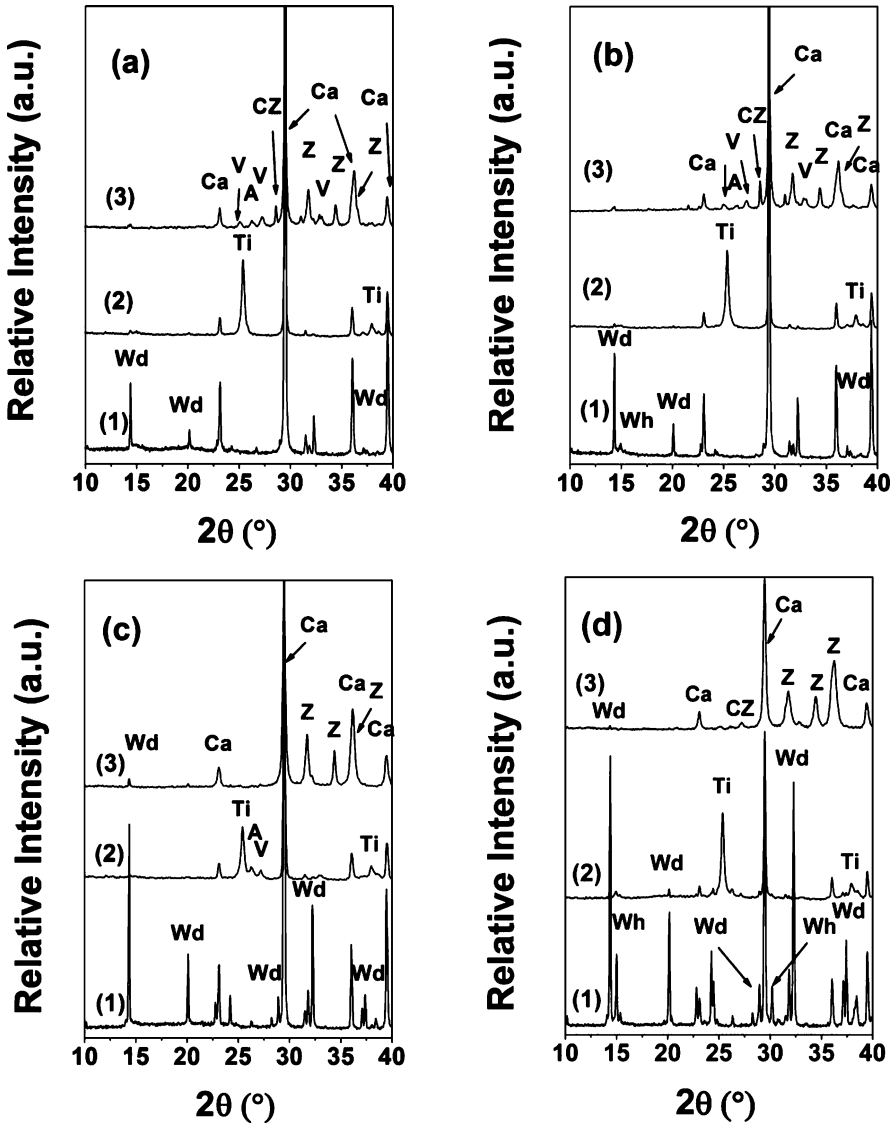

Figure 6. X-ray diffraction analysis of the limestone coupons using the Bragg–Brentano configuration before and 21 days after the inoculation with the two fungi under photoperiod conditions (D/NL). Limestone coupon A: (a) *A. niger*; (b) *P. oxalicum*. Limestone coupon B: (c) *A. niger*; (d) *P. oxalicum*. The three curves in each panel correspond to: (1) limestone coupon without antifungal coating; (2) with a $Ca(OH)_2$-50% TiO_2 coating; and (3) with a $Ca(OH)_2$-50% ZnO coating. The phases/materials observed were calcite (Ca), whewellite (Wh), weddellite (Wd), vaterite (V), aragonite (A), zincite (Z), calcium zincate dehydrate (CZ), and anatase (Ti).

observed for limestone coupon B with the $Ca(OH)_2$-50% TiO_2 coating inoculated with *P. oxalicum*, which indicates that the antifungal coating is not completely effective for this particular case. It can be concluded that the main results from XRD analysis agree with the visual antifungal activity measurements. The $Ca(OH)_2$-50% TiO_2 coating in general appears more effective from XRD analysis, while the slight ineffectiveness of the $Ca(OH)_2$-50% ZnO coating for limestone coupon B with *A. niger* was not observed with the visual inspection method. An interesting observation is the difference between interaction of the $Ca(OH)_2$ coating material with either ZnO or TiO_2 with the limestone: for the $Ca(OH)_2$-50% ZnO coating, a variety of calcium oxide phases are formed, including vaterite (V), aragonite (A), and calcium zincate dehydrate (CZ), whereas for the $Ca(OH)_2$-50% TiO_2 coating, only calcite is formed.

In summary, from the visual inspection it appears that the higher porous limestone A is somewhat less well protected from fungal colonization than limestone B, however, XRD analysis appears to result in the opposite trend. The XRD method gives a spatial average result and analyzes the material up to a depth of a few micrometers at most, while visual inspection tends to focus on surface anomalies; hence, the two methods analyze the samples in a different manner. It appears that the compositional differences between limestone A and B may be responsible for the difference in susceptibility for fungal attack, with limestone type B being more prone to attack according to the XRD results, in agreement with the results shown in Figure 6.

To determine the influence of limestone and coating morphologies on localized fungal attack, the colonization morphology was inspected by SEM both before and after the coatings were applied to the limestone coupons, which is shown in Figures 7 and 8. Two types of colonization growth were observed for both types of limestone: (i) on the surface of the limestone coupon and, (ii) in the subsurface region, penetrating the substrate. *P. oxalicum* colonies show a flat,

dx.doi.org/10.1021/am302783h | *ACS Appl. Mater. Interfaces* 2013, 5, 1556–1565

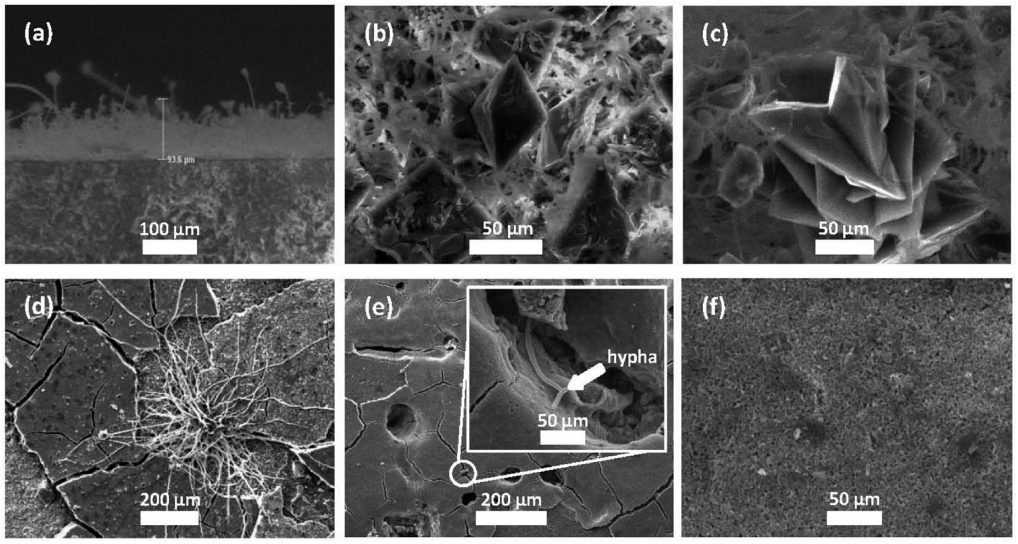

Figure 7. (a) Transversal cut side view of the surface of limestone coupon A with *A. niger*. (b) Crystals of calcium oxalate dihydrate (weddellite) on coupon B with *P. oxalicum*. (c) Crystals of calcium oxalate monohydrate (whewellite) on coupon B with *P. oxalicum*. (d) Coupon B with the protective layer of TiO_2 and colonized with *A. niger*. (e) Coupon A with the protective layer of $Ca(OH)_2$-50% TiO_2 and colonized with *P. oxalicum*. (f) Coupon A with the protective layer of $Ca(OH)_2$-50% ZnO and colonized with *A. niger*..

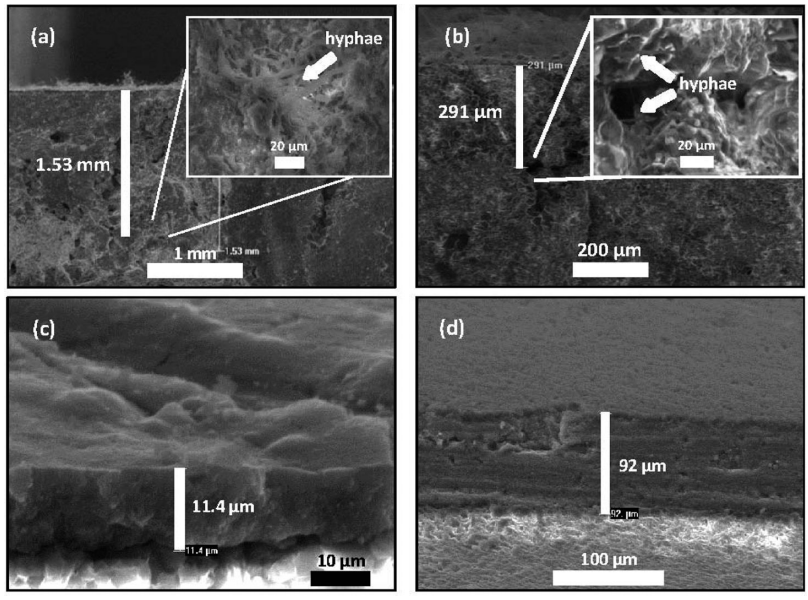

Figure 8. Cross-sectional images of limestone coupons showing hyphae penetration with *A. niger*; the penetration depths were determined to be: (a) 1.53 mm for coupon A; (b) 290 μm for coupon B. (c) Coupon B coating with TiO_2; (d) coupon B coating with $Ca(OH)_2$-50% ZnO.

filamentous, and velvet texture, where conidiophores, phialides, and branched conidia were identified. Images a and d in Figure 7 illustrate that *A. niger* has a high production of simple conidiophores hyalines with a globose vesicule at the apex, in which the black spores are observed. For limestone coupon B, larger amounts of spores were observed compared to limestone coupon A for both *A. niger* and *P. oxalicum*. Figure 7b shows the well-defined calcium oxalate crystals with a bipyramidal shape (with a 10 μm size) corresponding to weddellite, in agreement with the results from X-ray diffraction and previous reports in the literature.[52,54,55] In Figure 7c, whewellite crystals are observed, corresponding to the interaction between limestone coupon B and *P. oxalicum*. All coatings show favorable antifungal results.

Images d and e in Figure 7 show limestone samples covered with a TiO_2 and $Ca(OH)_2$-50% TiO_2 coating, respectively: an important observation is that the coatings were not homogeneous and showed larger pores and cracks, and in these regions, some fungal growth can be observed. In addition, the coatings were somewhat fragile and were easily removed. On the other hand, the ZnO and $Ca(OH)_2$-50% ZnO coatings showed a more homogeneous, better adhered layer to the limestone materials. As a consequence, as shown in Figure 7f, fungal growth was not observed for these coating materials.

A transversal cut was made in order to analyze the hyphae penetration in the subsurface of the limestone coupons, as illustrated in Figure 8. The mean thickness of the coupons was around 2.3 mm, and when the natural limestone coupons without the coatings were inoculated, the thickness of the

colonized biofilms on top of the limestone coupon surface was around 93 and 60 μm, for *A. niger* and *P. oxalicum*, respectively. In Figure 8a, a cross-sectional image reveals that the hyphae of *A. niger* on limestone coupon A can penetrate deeply into the material, and a depth of 1.53 mm is indicated in the image for one particular example. For limestone B, the penetration depth is generally much smaller, and the SEM image in Figure 8b shows an example of a 290 μm penetration depth. The same trends were observed for the mycelium penetration upon inoculating the limestone coupons A and B with *P. oxalicum*. These results clearly show the effect of stone porosity on the susceptibility for fungal attack: although the visual inspection method of the surface and the averaging method of X-ray diffraction seemed to indicate that limestone B was more susceptible to fungal deterioration, most likely related to a different mineralogical composition, the SEM images demonstrate that the more porous limestone A is more prone to fungal deterioration up to much greater depths. It has been found that fungi are able to penetrate up to a depth of 4 to 9 mm, through cracks and microfissures of rock samples in stone buildings after 6 months of culture.[51] In summary, limestone A has a higher porosity, hence, a high incidence of fractures and cavities was generally present, leading to more pronounced hyphae penetration. In addition, because the TiO_2-based coatings were characterized by a higher incidence of cracking, their performance in terms of hyphae penetrations was generally worse than for the ZnO-based coatings.

Images c and d in Figure 8 show cross-sectional images of the limestone B samples with antifungal coatings: the thickness of the TiO_2 coating is about 11 μm, while the thickness of the $Ca(OH)_2$-50% ZnO film is about 90 μm. The increase in coating thickness in the presence of $Ca(OH)_2$ and ZnO is related to the interaction between the $Ca(OH)_2$ material and the limestone (see Table S1 in the Supporting Information for the complete results). On the other hand, for the mixed system with TiO_2, this effect is not observed related to the difference in basicity of the two materials. In addition, it was found that the coating thickness was larger for limestone A, which may be related to its larger porosity resulting in a better anchoring of the antifungal coating. It can be concluded that it is desirable to have $Ca(OH)_2$ as a base material for ZnO antifungal coatings because of its excellent compatibility with the limestone surfaces.

4. CONCLUSIONS

Protective coatings of $Ca(OH)_2$, either pure or mixed with ZnO or TiO_2 nanoparticles, on glass slides and on limestone coupons have antifungal properties, leading to growth inhibition of *Penicillium oxalicum* and *Aspergillus niger*. Experiments were carried out at a laboratory test site in the dark and under simulated photoperiod conditions, consisting of 24-h cycles of 12 h in the dark and 12 h under illumination. It was observed that in vitro fungal growth inhibition on glass slides with the $Ca(OH)_2$-*x*ZnO and pure zincite antifungal coatings was effective both in the dark and under simulated photoperiod conditions. On the other hand, TiO_2-based treatments were practically noneffective in terms of antifungal activity in the dark, and although under simulated photoperiod conditions the antifungal activity of $Ca(OH)_2$-*x*TiO_2-based coatings improved, the coatings were not fully effective according to the visual inspection method. X-ray diffraction was used to investigate the interaction between the fungi and the $Ca(OH)_2$-based protective coatings, and it was found that the formation of the calcium oxalates weddelite and whewellite can be used as an indicator of the fungal activity.

The antifungal properties were evaluated on two limestone coupons coated with TiO_2, $Ca(OH)_2$-50% TiO_2, ZnO, and $Ca(OH)_2$-50% ZnO. The limestone coupons were collected from quarries on the Yucatán peninsula: limestone type A is a more porous material than limestone type B, and there are also significant differences in the mineralogical composition. After 21 days of inoculation and exposure to photoperiod conditions, a moderate antifungal activity was observed for *A. niger* for both limestone types with the TiO_2 and $Ca(OH)_2$-50% TiO_2 coatings, whereas an effective behavior was observed for *P. oxalicum* with TiO_2 and $Ca(OH)_2$-50% TiO_2 coatings. For ZnO and $Ca(OH)_2$-50% ZnO coatings on both stones and with both fungi an effective antifungal activity was observed. X-ray diffraction studies indicate that the TiO_2-based coatings appear effective, except for limestone B with *P. oxalicum*, whereas the ZnO-based coatings are effective, except for a limestone B with *A. niger* where a small amount of weddelite was observed. Hence, from X-ray diffraction it can be concluded that limestone B is somewhat more prone to fungal attack than limestone A, related to the differences in mineralogical content. On the other hand, close inspection of samples with SEM revealed that fungal penetration into the limestone material was more pronounced for limestone type A, which is more porous. SEM images also show that the TiO_2-based coatings are less homogeneous and have more cracks than the ZnO-based coatings, which was reflected in a much better antifungal behavior of the ZnO-based coatings. These results illustrate that apart from the antifungal properties of the materials, also the morphological properties of the protective coatings are important for their effectiveness. Hence, to fully characterize the antifungal properties of protective coatings, it is essential to apply various evaluation methods.

■ ASSOCIATED CONTENT

Ⓢ Supporting Information

Figure S1 shows a semiquantitative X-ray analysis illustrating the phase formation related to the interaction of fungi and coatings on glass slides. Figure S2 shows a semiquantitative analysis of the XRD spectra for the limestone samples with the four different antifungal coatings. Figure S3 shows an SEM image of the hyphae formed with *A. niger* on limestone coupon B illustrating that calcium oxalate crystals are found in the biofilm, indicating that the biomineral is formed by the fungus from organic acids and calcium ions released by the limestone. Table S1 shows the thickness of the antifungal coatings on the limestone coupons A and B, respectively, as obtained from cross-sectional SEM images. This material is available free of charge via the Internet at http://pubs.acs.org/.

■ AUTHOR INFORMATION

Corresponding Author

*E-mail: ngomez@mda.cinvestav.mx; nikte.m.g.o@gmail.com.

Notes

The authors declare no competing financial interest.

■ ACKNOWLEDGMENTS

The authors acknowledge CONACyT for financial support through projects LAB-123913 and FOMIX-Yucatan 108528, 108160. We are grateful to D. Aguilar and D. Huerta for their valuable technical support.

REFERENCES

(1) Ortega-Morales, B. O.; Gaylarde, C. C.; Englert, G. E.; Gaylarde, P. M. *Int. Biodeterior. Biodegrad.* **2006**, *58*, 19−123.
(2) Gaylarde, C.; Ortega-Morales, B. O.; Bartolo, P. *Curr. Microbiol.* **2007**, *54*, 162−166.
(3) Stjepko, G.; Friedmann, E. I.; Schneider, J. *J. Sediment. Res.* **1981**, *51*, 475−478.
(4) Ortega-Morales, B. O.; Gaylarde, C. C.; Englert, G. E.; Gaylarde, P. M. *J. Geomicrobiol.* **2005**, *22*, 261−268.
(5) Ortega-Morales, B. O.; Narváez-Zapata, J. A.; Schmalenberger, A.; Sosa-López, A.; Tebbe, C. C. *Biofilms* **2004**, *1*, 79−90.
(6) Warscheid, T.; Braams, J. *Int. Biodeterior. Biodegrad.* **2000**, *46*, 343−368.
(7) Lopez-Arce, P.; Gomez-Villalba, L. S.; Pinho, L.; Fernández-Valle, M. E.; Álvarez de Buergo, M.; Fort, R. *Mater. Charact.* **2010**, *61*, 168−184.
(8) Gadd, G. M. *Mycol. Res.* **2007**, *111*, 34−9.
(9) Macedo, M. F.; Miller, A. Z.; Dionísio, A.; Saiz-Jimenez, C. *Microbiol.* **2009**, *155*, 3476−3490.
(10) De la Rosa-García, S. C.; Ortega-Morales, B. O.; Gaylarde, C. C.; Beltrán-García, M. J.; Quintana-Owen, P.; Reyes-Estebanez, M. *Rev. Mex. Micol.* **2011**, *33*, 43−51.
(11) Eckhardt, F. E. W. In *6th International Congress on Deterioration and Conservation of Stone*; Ciabach, J., Ed.; Nicholas Copernicus University Press Department: Torun, Poland, 1988; Vol. 2, pp 71−81.
(12) Wilson, M. J.; Jones, D. In *Residual Deposits: Surface Related Weathering Processes and Materials (Geological Society Special Publication)*; Blackwell: London, 1983; pp 5−12.
(13) Kumar, K.; Kumar, A. V. *Biodeterioration of Stone in Tropical Environments. An Overview*; Research in Conservation Series; The Getty Conservation Institute, Los Angeles, 1999; pp 29−31.
(14) Scheerer, S.; Ortega-Morales, B. O.; Gaylarde, C. C. *Adv. Appl. Microbiol.* **2009**, *66*, 97−139.
(15) Tiano, P.; Cantisani, E.; Sutherland, I.; Paget, J. M. *J. Cult. Herit.* **2006**, *7*, 49−55.
(16) Fonseca, A. J.; Pina, F.; Macedo, M. F.; Leal, N.; Romanowska-Deskins, A.; Laiz, L.; Gómez-Bolea, A.; Saiz-Jimenez, F. *Int. Biodeterior. Biodegrad.* **2010**, *64*, 388−396.
(17) Baglioni, P.; Giorgi, R. *Soft Matter* **2006**, 293−303.
(18) Dei, L.; Salvadori, B. *J. Cult. Herit.* **2006**, *7*, 110−115.
(19) Blee, A.; Matisons, J. G. *Mater. Forum* **2008**, *32*, 121−128.
(20) Ambrosi, M.; Dei, L.; Giorgi, R.; Neto, C.; Baglioni, P. *Langmuir* **2001**, *17*, 4251−4255.
(21) Rodriguez-Navarro, C.; Ruiz-Agudo, E.; Ortega-Huertas, M.; Hansen, E. *Langmuir* **2005**, *21*, 10948−10957.
(22) Daniele, V.; Taglieri, G.; Quaresima, R. *J. Cult. Herit.* **2008**, *11*, 294−301.
(23) Daniele, V.; Taglieri, G. *J. Cult. Herit.* **2010**, *11*, 102−106.
(24) Hirota, K.; Sugimoto, M.; Kato, M.; Tsukagoshi, K.; Tanigawa, T.; Sugimoto, H. *Ceram. Int.* **2010**, *36*, 497−506.
(25) Panigrahi, J.; Behera, D.; Mohanty, I.; Subudhi, U.; Nayak, B. B.; Acharya, B. S. *Appl. Surf. Sci.* **2011**, *258*, 304−311.
(26) Yamamoto, O.; Shimura, T.; Sawai, J.; Kojima, H.; Sasamoto, T. *JCS Jpn.* **2000**, *108*, 156−180.
(27) Sawai, J.; Yoshikawa, T. *J. Appl. Microbiol.* **2004**, *96*, 803−809.
(28) Zhou, J.; Xu, N.; Wang, Z. L. *Adv. Mater.* **2006**, *18*, 2432−2435.
(29) Huh, A. J.; Kwon, Y. J. *J. Controlled Release* **2011**, *156*, 128−145.
(30) Dastjerdi, R.; Montazer, M. *Coll. Surf. B* **2010**, *79*, 5−18.
(31) He, L.; Liu, Y.; Mustapha, A.; Lin, M. *Microbiol. Res.* **2011**, *166*, 207−215.
(32) Padmavathy, N.; Vijayaraghavan, R. *Sci. Technol. Adv. Mater.* **2008**, *9*, 1−7.
(33) Lin, H.-M.; Keng, C.-H.; Tung, C.-Y. *Nanostruct. Mater.* **1997**, *9*, 747−750.
(34) Mo, S.-D.; Ching, W. Y. *Phys. Rev. B* **1995**, *51*, 13023−13032.
(35) Chen, J.; Poon, C. *Build. Environ.* **2009**, *44*, 1899−1906.
(36) Heredia-Cervera, B. E.; González-Azcorra, S. A.; Rodríguez-Gattorno, G.; López, T.; Ortiz, E. A.; Oskam, G. *Sci. Adv. Mater.* **2009**, *1*, 63−68.
(37) Grätzel, M.; O'Regan, B. *Nature* **1991**, *354*, 737−740.
(38) Diamanti, M. V.; Ormellese, M.; Pedeferri, M. *Cem. Concr. Res.* **2008**, *38*, 1349−1353.
(39) Fonseca, A. J.; Pina, F.; Macedo, M. F.; Leal, N.; Romanowska-Deskins, A.; Laiz, L.; Gómez-Bolea, A.; Saiz-Jimenez, C. *Int. Biodeterior. Biodegrad.* **2010**, *64*, 388−396.
(40) Burnside, S. D.; Shklover, V.; Barbé, C.; Comte, P.; Arendse, F.; Brooks, K.; Grätzel, M. *Chem. Mater.* **1998**, *10*, 2419−2425.
(41) Cullity, B. D. *Elements of X-ray Diffraction*; Addison-Wesley:, Reading, MA, 1978; Vol. 2, pp 81−106.
(42) Langford, J. I.; Wilson, A. J. C. *J. Appl. Crystallogr.* **1978**, *11*, 102−113.
(43) Burford, E. P.; Hillier, S.; Gadd, M. G. *Geomicrobiology* **2006**, *23*, 599−611.
(44) Gómez-Cornelio, S.; Mendoza-Vega, J.; Gaylarde, C. C.; Reyes-Estebanez, M.; Morón-Ríos, A.; De la Rosa-García, S C.; Ortega-Morales, B. O. *Fungal Biol.* **2012**, 1−12.
(45) Fonseca, A. J.; Pina, F.; Macedo, M. F.; Leal, N.; Romanowska-Deskins, A.; Laiz, L.; Gomez-Bolea, A.; Saiz-Jimenez, C. *Int. Biodeterior. Biodegrad.* **2010**, *64*, 388−396.
(46) Mukhpadhyab, A.; Basak, S.; Kishore-Das, J.; Kumar-Medda, S.; Chattopadhyay, K.; De, G. *ACS Appl. Mater. Interfaces* **2010**, *2* (9), 2540−2546.
(47) Chen, J.; Poon, C.-S. *Build. Environ.* **2009**, *44*, 1899−1906.
(48) Matteini, M. *Conserv. Sci. Cult. Herit.* **2008**, *8*, 13−27.
(49) Trezza, M. A. *Mater. Res.* **2007**, *10* (4), 331−334.
(50) Lin, T.-C.; Yousuf Mollah, M. A.; Rajav Vempati, K.; Cocke., D. L. *Chem. Mater.* **1995**, *7* (10), 1974−1978.
(51) May-Crespo, J.; Martínez-Torres, P.; Alvarado-Gil, J. J.; Quintana, P.; Vilca-Quispe, L. *Int. J. Thermophys.* **2012**, *33*, 1908−1915.
(52) de la Torre, M. A.; Gomez-Alarcon, G.; Palacios, J. M. *Appl. Microbiol. Biotechnol.* **1993**, *40*, 408−415.
(53) ASTM D2216−98. *Standard test Method for Laboratory Determination of Water (Moisture) Content of Soil and Rock by Mass*; ASTM International: West Conshohocken, PA, 2007.
(54) Guiordani, P.; Modenesi, P.; Tretiach, M. *Lichenologist* **2003**, *35* (3), 255−270.
(55) Osterrieth, M. L.; Oyarbide, F.; Bordas, V. *Ciencia Suelo* **2000**, *18* (1), 50−58.